RSC Advances

PAPER

View Article Online
View Journal | View Issue

Cite this: *RSC Adv.*, 2024, **14**, 30924

Novel pyridine isonicotinoyl hydrazone derivative: synthesis, complexation and investigation for decontamination of DR-81 from wastewater

Mohamed A. Ahmed,[a] Eslam Salama, *[b] M. H. H. Mahmoud,[c] Mohamed Ebaid[d] and Mohamed A. Khalifa *[a]

Herein, novel aroylhydrazone (*E*/*Z*)-*N*′-((3-methylpyridin-2-yl)methylene)isonicotinohydrazide ligand (MPIH) **3** and its Zn(II)-MPIH complex **4** were synthesized and investigated to adsorb direct red 81 dye (DR-81) from aqueous media. MPIH was synthesized by the condensation reaction of isonicotinohydrazide with 3-methylpicolinaldehyde **2**, then performed in a basic medium with zinc chloride to form Zn(II)-MPIH complex. The synthesized MPIH ligand **3** and Zn(II)-MPIH complex **4** were further characterized *via* proton nuclear magnetic resonance (^{1}H NMR), ^{13}C nuclear magnetic resonance, Fourier transform infrared spectroscopy (FT-IR), UV-visible, mass spectra analysis (EI MS), and elemental analysis. The synthesized MPIH ligand **3** and Zn(II)-MPIH complex **4** were evaluated for their ability to decontaminate DR-81 from wastewater. The performance of MPIH ligand **3** to adsorb DR-81 from wastewater was lower than Zn(II)-MPIH complex **4** over contact times of 180 minutes. The optimal dosage of the Zn(II)-MPIH complex **4** was determined to be 1.0 g L^{-1} at pH 7, achieving 88.3% adsorption of 10 ppm DR-81 within 45 minutes. Thermodynamic analysis showed that the decontamination process was spontaneous and exothermic when using the fabricated Zn(II)-MPIH complex **4**. The kinetic parameters aligned well with the pseudo-second-order kinetics model, and the adsorption process was accurately described by the Freundlich isotherm. The adsorption data confirmed that the Zn(II)-MPIH complex **4** is an effective adsorbent for DR-81 in aqueous solutions, demonstrating high stability, the ability to be recycled for up to seven cycles, and ease of regeneration.

Received 7th August 2024
Accepted 23rd September 2024

DOI: 10.1039/d4ra05731g

rsc.li/rsc-advances

1. Introduction

Water is essential for all forms of life and is a critical resource for maintaining the health and well-being of ecosystems, human societies, and economies. As global populations grow and climate change alters water availability and distribution, managing this precious resource sustainably is more important than ever to ensure the prosperity and survival of future generations.[1] Water contamination is a critical global issue that arises from the introduction of harmful substances into water bodies, threatening both human health and the environment.[2] Industrial activities, agricultural runoff, and improper waste disposal are significant contributors to water pollution.[3] Among the various contaminants, dyes from industries like textiles, paper, and plastics are particularly concerning due to their synthetic nature, non-biodegradability, and resistance to environmental degradation. Additionally, many dyes contain toxic compounds that can pose serious health risks to humans and aquatic life, including carcinogenic effects and bioaccumulation in the food chain.[4]

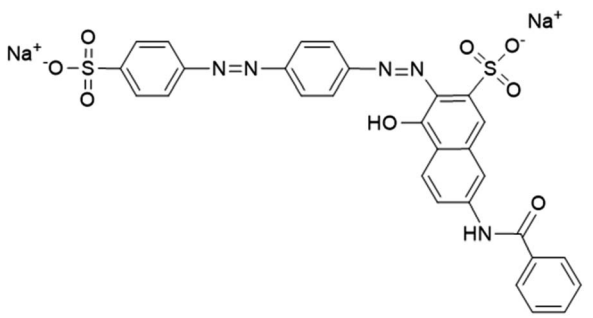

Fig. 1 The chemical structure of Direct Red-81.

[a]*Chemistry Department, Faculty of Science, Damanhour University, Damanhour 22511, Egypt. E-mail: mohamed-ali@sci.dmu.edu.eg; mohamed-khalifa@sci.dmu.edu.eg*

[b]*Environment and Natural Materials Research Institute (ENMRI), City of Scientific Research and Technological Applications (SRTA-City), New Borg El-Arab City, Alexandria 21934, Egypt. E-mail: esalama@srtacity.sci.eg*

[c]*Department of Chemistry, College of Science, Taif University, P.O. Box 11099, Taif, 21944, Saudi Arabia. E-mail: mheshamm@tu.edu.sa*

[d]*Plant Production Department, Arid Lands Cultivation Research Institute (ALCRI), City of Scientific Research and Technological Applications (SRTA-City), New Borg El-Arab City, Alexandria, 21934, Egypt. E-mail: mohamedebaid979@gmail.com*

Contamination of water by Direct Red 81 (DR-81), (3E)-7-benzamido-4-oxo-3-[[4-[(4-sulfonatophenyl)diazenyl]phenyl] hydrazinylidene] naphthalene-2-sulfonate (Fig. 1), which is a sulfonated azo dye used extensively in the textile and paper industries, poses significant environmental risks. DR-81 is a synthetic dye known for its vibrant red color, high solubility in water, and stability under various pH conditions, which, combined with its resistance to biodegradation, allows it to persist in water bodies for extended periods and makes it commonly used in various industrial applications and textiles.[5] When released into aquatic environments through industrial wastewater, DR-81 can impart a vivid color to the water, reducing light penetration and thereby affecting photosynthesis in aquatic plants, which disrupts the entire aquatic food chain. Additionally, DR-81 can produce harmful byproducts upon degradation, some of which are known to be toxic, mutagenic, and potentially carcinogenic.[6] These substances can bioaccumulate in aquatic organisms, leading to long-term health risks for both marine life and humans who consume contaminated water or seafood. The presence of DR-81 in water can also affect physical and chemical properties of the water, making it unfit for recreational and domestic use. The environmental impact of DR-81 underscores the urgent need for effective treatment methods to remove such contaminants from industrial effluents and to implement stricter regulatory measures to prevent their release into the environment.[7]

The adsorption of DR-81 dye from wastewater is a widely studied approach for mitigating its environmental impact, and numerous techniques and materials have been explored for this purpose.[8] Adsorption is favored due to its simplicity, cost-effectiveness, and high efficiency in removing dyes from aqueous solutions. Various adsorbents have been developed, ranging from conventional activated carbon to innovative materials like metal–organic frameworks (MOFs), biochar, and nanocomposites.[5,7,9] Activated carbon is a popular choice due to its large surface area and porous structure, which facilitates the adsorption of dye molecules.[4] However, researchers are increasingly investigating alternative materials to improve adsorption capacity and reduce costs. For instance, biochar derived from agricultural waste has gained attention for its sustainability and effectiveness in adsorbing dyes. Additionally, metal oxides and nanocomposites, such as those containing graphene oxide or magnetic nanoparticles, offer enhanced adsorption properties and the potential for easy separation from treated water.[4] Advanced techniques like surface modification of adsorbents and the use of hybrid materials have further improved the adsorption efficiency of DR-81.[9] These innovations contribute to the development of more sustainable and efficient wastewater treatment methods, addressing the challenge of dye contamination in water systems.

Hydrazone derivatives are one of the most important types of flexible and adaptable polydentate ligands, having a high chelating efficacy with transition metal ions.[10,11] The nucleophilic nature of the nitrogen atoms in the triatomic structure C=N–N of the azomethine group makes hydrazones able to coordinate.[12,13] Researchers have been paying close attention to hydrazone-based metal complexes in a variety of applications, such as chromogenic reagents for the spectrophotometric detection of transition-metal ions, metal extracts, and physiologically active substances. They have also been demonstrated to possess diverse biological applications,[14] nonlinear optics properties,[15] adsorption properties,[16] analytical applications,[17] catalytic applications,[18] electrochemical properties,[19] and luminescent properties.[20] Considering different hydrogen bond interactions, nonclassical hydrogen bond interactions, and porous structures in the hydrazone complexes, those complexes have the ability to adsorb gas and alcohol vapor.[21,22] The Langmuir surface area and BET (Brunauer–Emmett–Teller) surface area for complexes were determined, which decreased in the following order: Cu(II) > Cd(II) > Hg(II) > Zn(II). The adsorption isotherms show a typical type III nature, with the largest quantities adsorbed for complexes Cu(II), Cd(II), Hg(II), and Zn(II) being 7.81, 5.59, 6.36, and 6.72 mmol g^{-1} respectively. It is meaningful for the complexes to be potential materials as adsorbents of methanol vapor.[16] Also, the vapor adsorption isotherms of metal ions Hg(II), and Cd(II) with two organic ligands 3-amino-*N*′-(1-(pyridin-4-yl)ethylidene)benzohydrazide (L^1) and 3-amino-*N*′-(1-(pyridin-3-yl)ethylidene)benzohydrazide (L^2) were obtained by a Micromeritics ASAP 2020 system under the methanol vapor atmosphere. The samples were activated at 373 K for 8 hours until the outgassing rate was less than 4 mmHg min^{-1}. The Langmuir surface area and BET (Brunauer–Emmett–Teller) surface area for complexes were determined, which decreased in the following order: Hg(II)-L^1 > Cd(II)-L^1 > Cd(II)-L^2 > Hg(II)-L^2.[23]

The novel pyridine isonicotinoyl hydration derivative represents a promising advancement in the field of wastewater treatment, particularly for the removal of synthetic dyes like DR-81. This compound, characterized by its unique structural properties, offers enhanced interaction with dye molecules through multiple binding sites, promoting efficient adsorption.[24] The presence of pyridine and isonicotinoyl groups provides a robust framework for complexation, allowing for greater stability and reactivity in aqueous environments. Unlike conventional adsorbents, this derivative exhibits high specificity and capacity for DR-81, making it a potentially superior alternative for decontamination processes.[10] The innovation lies in its ability to address the challenges associated with dye pollution, such as the need for rapid adsorption kinetics and minimal secondary pollution, thereby offering a sustainable and efficient solution for industrial effluent treatment. In this study, we present the synthesis and complexation of a novel pyridine isonicotinoyl hydrazone derivative, exploring its potential as an efficient adsorbent for the decontamination of DR-81 dye from wastewater. The increasing release of synthetic dyes like DR-81 into aquatic systems has raised significant environmental concerns due to their persistence, toxicity, and resistance to biodegradation. This work aims to address these challenges by investigating the adsorbent's efficacy through a comprehensive analysis of various parameters such as adsorption capacity, adsorbent dosage, and pH influence. The results of this study contribute to the growing body of research on wastewater treatment, providing insights into the

development of more effective and sustainable methods for removing hazardous dyes from contaminated water sources.

2. Results and discussion

2.1 Synthesis of (*E*/*Z*)-*N*′-((3-methylpyridin-2-yl)methylene) isonicotinohydrazide (MPIH) 3

The isoniazid compound **1** was synthesized by the known literature method (MP = 169–171 °C).[25] The condensation reaction of isonicotinohydrazide **1** with 3-methyl-picolinaldehyde **2** in methanol under refluxing produced the novel hydrazone derivative (MPIH) **3** (Scheme 1).

By using ^{1}H NMR, ^{13}C NMR, IR, UV, and elemental analysis, the structure of the ligand MPIH **3** was verified. The ^{1}HNMR of the ligand displays three sets of signals (Fig. 2a), indicating the presence of three species in solution: (*E*)-ketoamine, (*E*)-enamine, and (*Z*)-ketoamine (Scheme 2).[26] Because there are two cases of magnetic equivalency, each of the three systems can be observed to have 10 different resonances corresponding to the molecule's 12 hydrogens. Three methyl groups at 2.56, 2.52 ppm (in a 2 : 1 ratio), 21 aromatic protons at 7.30–8.90 ppm, and three azomethine groups (at 8.52, 7.62 ppm) are shown by ^{1}HNMR.[24,26] The existence of two methyl signals at 2.56, 2.52 ppm with a 2 : 1 ratio suggests the presence of ligand **3** in two forms, *E* and *Z* (2 : 1).[24,26] The occurrence of *Z* isomers in these structures could be attributed to the formation of an intramolecular hydrogen bond between the amide proton and the nitrogen of the pyridine ring, which leads to a low field shift in ^{1}H NMR spectra.[27] The N–H (ketoamines) or O–H (enamine) nuclei are associated with the ^{1}H spectrum's most deshielded signals. Due to the interaction of N–H with the solvent, the (*E*)-keto-amine isomer's signal is observed at 12.18 ppm, with a small overlap of the O–H signal of its (*E*)-enamine tautomer (broad at 12.13 ppm). On the other hand, the *N*–H···Npyr intramolecular hydrogen bond (Scheme 2) formed in the (*Z*)-keto-amine isomer gives the greatest deshielded signal, at 16.09 ppm.[24,26,27]

The ^{13}CNMR of ligand **3** (Fig. 2b), reveals a mixture of *E* and *Z* isomers. The existence of two methyl signals at chemical shifts 18.39 and 20.67 ppm with a ratio of 2 : 1 suggests the presence of ligand 3 in two forms: *E* and *Z*.[24] The appearance of 22 carbon signals in the range of 121.46–151.43 ppm indicates the presence of 20 aromatic carbons and 2 N=CH groups at 149.97–150.11 ppm.[28] Furthermore, the presence of a mixture of *E* and *Z* isomers is confirmed by the development of three signals at 162.00, 162.27, and 169.18 ppm (keto and enolate groups).

2.2 Formation of Zn(II)-MPIH complex 4

In the basic medium (Et_3N), the solution of $ZnCl_2$ was stirred with MPIH **3** to afford Zn(II)-MPIH complex **4** (Scheme 3). The structure of complex **4** was confirmed by ^{1}H NMR, ^{13}C NMR, IR, UV, and mass spectra.

The ligand IR-spectra reveal significant bands (Fig. 3) at 1671, 1633, 1601, 996, and 682 cm^{-1}, corresponding to ν(C=O), ν(C=N), ν(C=N_{py}), ν(N–N) and in-plan deformation of pyridine ρ(py).[26,29] The presence of carbonyl groups is responsible for the band observed in the infrared spectra of MPIH **3** in its solid state at 1671 cm^{-1}. The shift can be explained by the aromatic system, conjugation with double bonds.[26] The hydrazone stabilizes the keto-tautomer group based on the existence of a strong signal indicating of C=O group vibrations and the absence of a band in the free ligand's spectrum that can be attributed to ν(=C–OH).[26] The signal is recorded at 1429 cm^{-1} as a result of the combined effect of the NH bond's deformation and the N–C=O group's stretching vibration mode. Bonding of the ligand to Zn(II) center has been suggested by carefully comparing IR spectra of the complexes with that of the free ligand. The ν(C=O) vibrational mode disappears from the FT-IR spectra of the complex, and appear two new bands ν(C–O) at 1358 cm^{-1}and ν(C=N) at 1646 cm^{-1} indicates that the ligand is deprotonated and coordinated to the metal ion in the complex through the enol tautomer.[30] The strong absorption at 1633 cm^{-1}, attributed to the ν(C=N) azomethine group in the ligand, shows a downward shift of the bands to 1615 cm^{-1}, indicating that the nitrogen of the azomethine group is bound to Zn metal ion.[18] The ν(C=N_{py}) band has shifted by 26 cm^{-1}, indicating that the ligand is coordinated through the 2-pyridyl nitrogen. Additionally, the low energy pyridine ring in-plane and out-of-plane vibrations observed in the spectrum of the ligand at 682 cm^{-1}, are shifted to higher frequencies in the case of complexes, which is a good indication of the coordination of the heterocyclic nitrogen to the metal center.[31,32] The ligand coordination is substantiated by two bands appearing at 593, 528 cm^{-1} for the complexes; these are mainly attributed to ν (M–O) and ν (M–N), respectively.[31]

The ability of hydrazone MPIH to form a complex with Zinc was proved by ^{1}H and ^{13}C NMR spectroscopy. The ^{1}H NMR spectrum of Zn(MPIH)$_2$ **4** shows that in solution (DMSO-d_6), the metal was coordinated with two deprotonated ligands in *E*-form, resulting in signals from 22 protons in the complex (Fig. 4a). Two methyl groups at 2.56, 2.57 ppm, 14 aromatic protons at 7.30–9.01 ppm and two azomethine groups (at 8.54–8.25 ppm) are shown by ^{1}HNMR. Similarly, the ^{13}C NMR

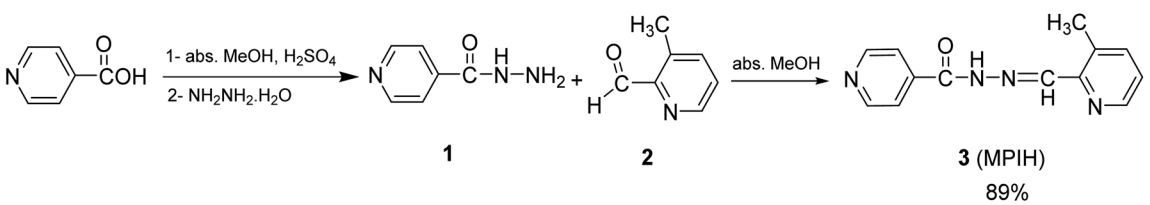

Scheme 1 Synthetic pathway for ligand MPIH **3**.

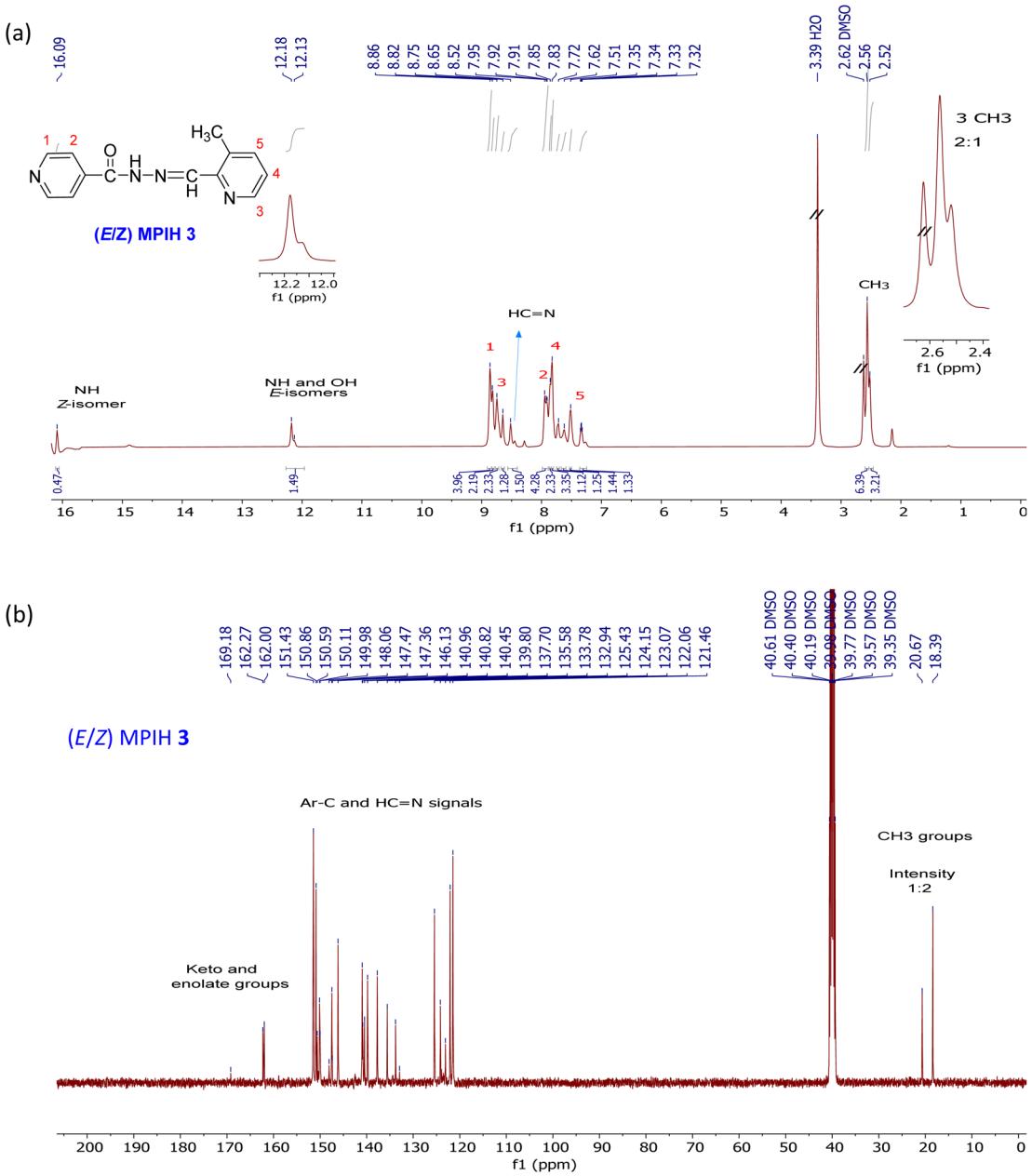

Fig. 2 ^{1}H NMR (a), ^{13}C NMR (b) spectrum of (*E*/*Z*)-*N*′-((3-methylpyridin-2-yl)methylene)isonicotinohydrazide (MPIH) **3**.

spectrum includes signals from 21 carbon atoms (Fig. 4c).[33] In DMSO-d_6, ^{1}H NMR of Zn(II)-MPIH complex showed changes compared with MPIH **3** signals (Fig. 4a and b). The N–H signal of the amide group at 12.1 ppm in the ^{1}H NMR of MPIH **3** disappeared in complex (Fig. 4a), the C=O signal (162.00 and 162.27 ppm) in the ligand's ^{13}C NMR similarly disappeared, and a new signal corresponding to the synthesis of the enolate group formed at 173.14 and 172.86 ppm indicating that the MPIH **3** is

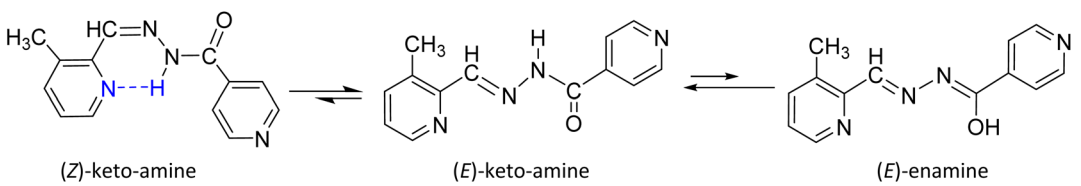

Scheme 2 Chemical forms of ligand MPIH **3** are present in a DMSO-d_6 solution at room temperature.

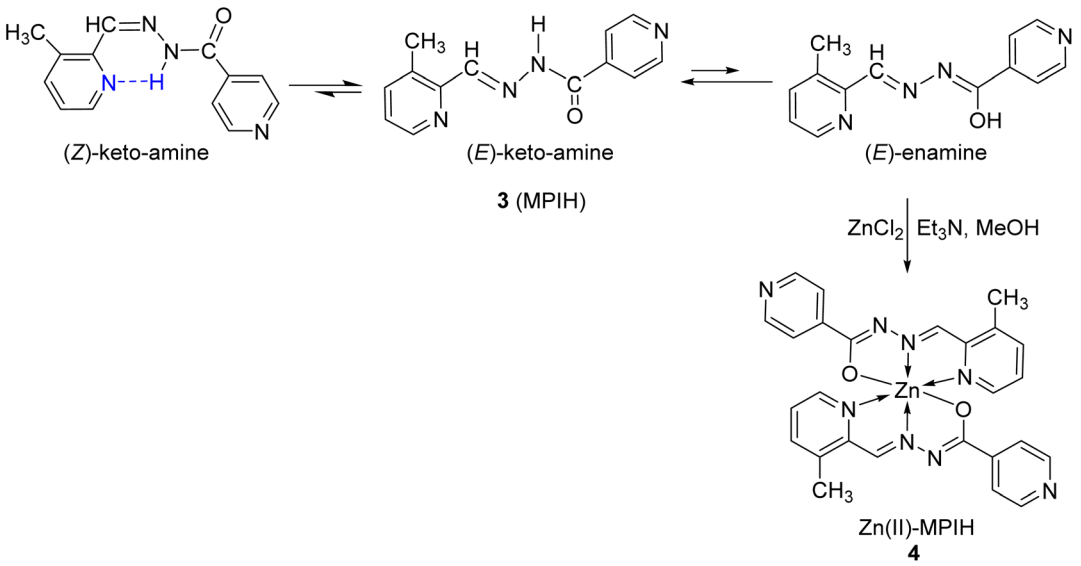

Scheme 3 Synthetic pathway for Zn(II)-MPIH complex 4.

coordinated in the enolic form (Fig. 4).[34,35] In addition, the Zn(II)-MPIH complex showed field shifts in the sp^2 protons. The largest shifts are observed for the aromatic proton of the pyridine ring ArH3 (proton 3 has $\Delta\delta = -1.01$ ppm), for the aromatic protons of the isoniazid ring ArH2 and ArH1 (protons ArH2 and ArH1 have $\Delta\delta = +0.08$, 0.07–1.00 ppm respectively) as well as the azomethine proton (–HC=N– proton has $\Delta\delta = -0.05$ ppm) while the proton signals ArH_4 and ArH5 are less shifted (have $\Delta\delta = 0.0$ and +0.01 ppm, respectively).[36] Thus, it becomes obvious that the hydrazone MPIH **3** is coordinated with zinc forming a Zn(II)-MPIH complex.

Electronic absorption bands of **3** and **4** (10^{-4} M) were recorded in methanol solution. UV-spectra of the ligand MPIH **3** exhibits two bands at 307 and 366 nm, caused by the π–π* and n–π* transitions of the pyridine ring and the azomethine group of the ligand (Fig. 5). The absorption maximum value of these bands exhibited a hyperchromic shift, which might be attributed to the donation of a lone pair of electrons to the metal as well as the conjugation created during complexation. No significant absorptions were observed above 400 nm, suggesting the absence of d–d bands, which is consistent with the d10 configuration of the Zn(II) ion.[37]

Mass spectra analysis (EI MS) was performed to confirm the existence of the complexes in the gas phase (Fig. 6). The EI MS spectra of Zn(II)-MPIH revealed that signals with m/z 480.59 correspond to $[(MPIH)_2]$ (calculated for $C_{26}H_{24}N_8O_2 = 480.20$) and m/z 542.32 correspond to $[Zn(MPIH)_2]$ (calculated for $C_{26}H_{22}N_8O_2Zn = 542.11$) and the base peak corresponds to $[C_{17}H_{19}O_2N_8Zn]$ (calculated/found (m/z) = 431.09, 431.42). These results indicate the formation of a mononuclear complex containing Zn(II) coordinated with two anionic hydrazone ligands.

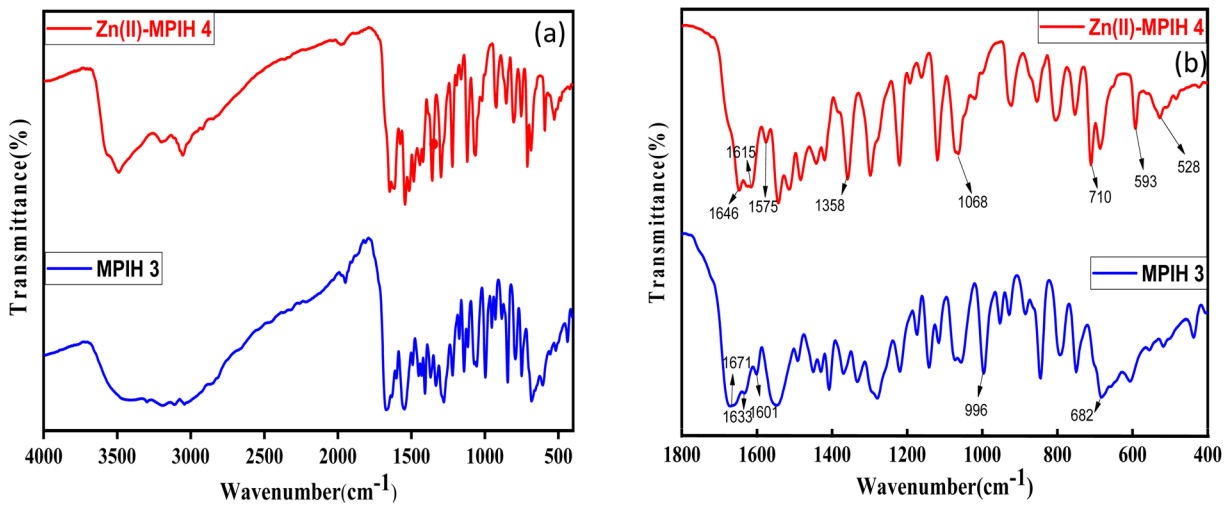

Fig. 3 (a) FTIR spectra of the ligand MPIH **3** and their complex **4** in the solid state, (b) selected region of the IR spectra of the solid-state MPIH **3** and their complex **4**.

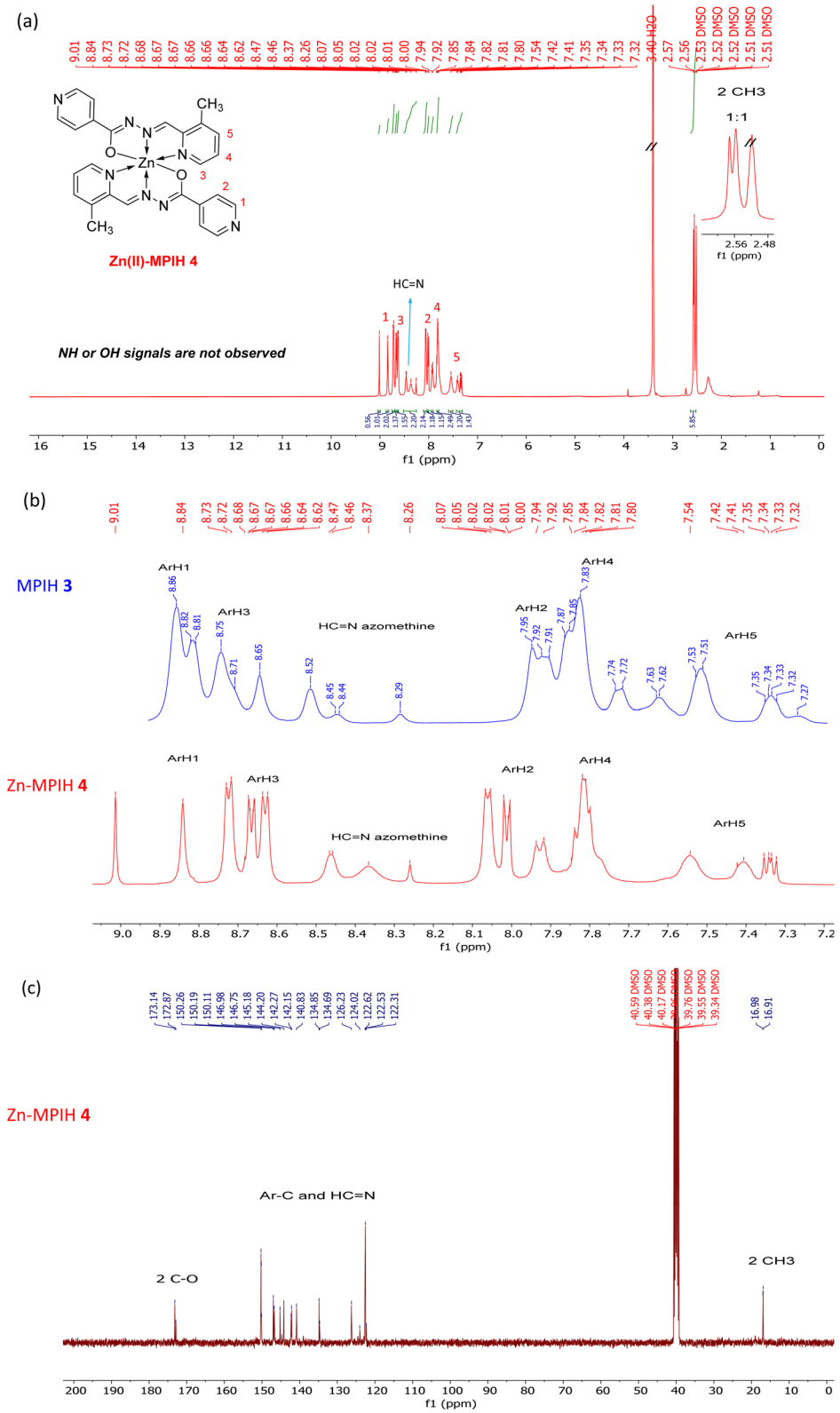

Fig. 4 (a) ^{1}H NMR of Zn(II)-MPIH complex **4**, (b) comparison between ^{1}H NMR chemical shifts of MPIH **3** protons and Zn(II)-MPIH **4** protons in the range 7.32–9.01 ppm and (c) ^{13}C NMR of Zn(II)-MPIH complex **4** in DMSO-d_6 at 25 °C.

2.3 Decontamination of DR-81 dye onto Zn(II)-MPIH

The feasibility of Zn(II)-MPIH was tested to remove DR-81 from wastewater *via* batch technique.

2.3.1 Kinetics of DR-81 adsorption onto MPIH and Zn(II)-MPIH. The adsorption of DR-81 onto the MPIH and Zn(II)-MPIH was examined over contact times of 180 minutes at various

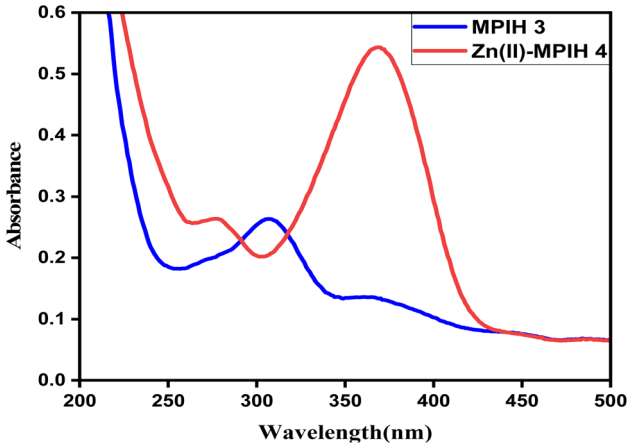

Fig. 5 Electronic absorption spectra of the ligand MPIH **3** and Zn(II)-MPIH complex **4**.

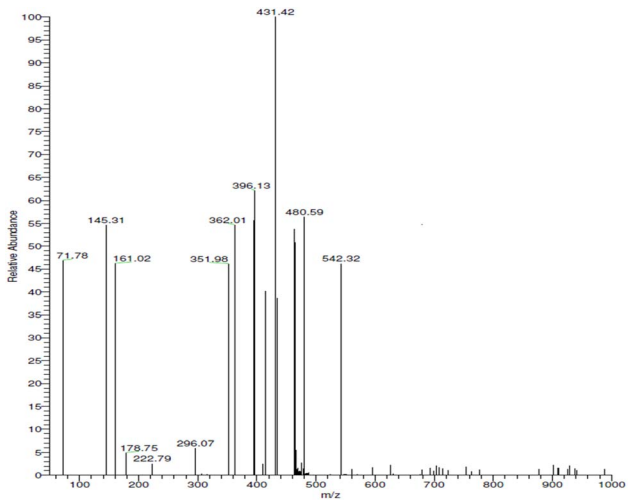

Fig. 6 EI MS of Zn(II)-MPIH complex **4**.

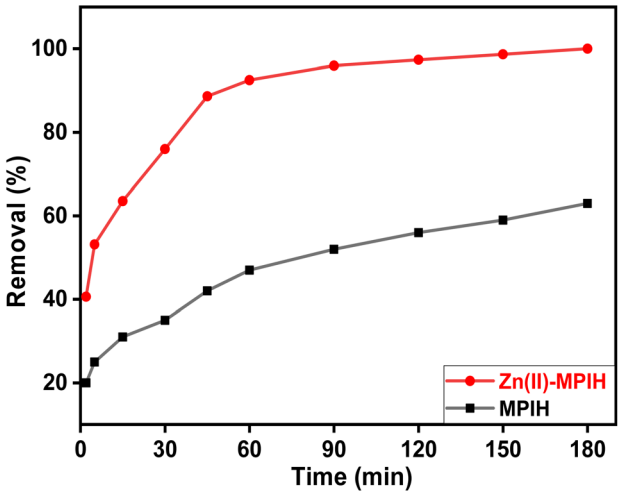

Fig. 7 Effect of contact time on DR-81 decontamination process onto Zn(II)-MPIH (pH = 7, material dosage = 1.0 g L^{-1}, initial DR-81 concentration = 10 ppm, stirring speed = 350 rpm and temperature = 25 °C).

intervals. As shown in Fig. 7, the initial adsorption of DR-81 onto the Zn(II)-MPIH occurs rapidly compared to the MPIH, attributed to the large surface area and functional groups present on the Zn(II)-MPIH material.[10,38] Following this initial phase, the adsorption rate slows until equilibrium is reached. This high adsorption efficiency may be due to the positively charged amino functional groups on the Zn(II)-MPIH, which interact with the DR-81 molecules.[7,10,39] The equilibrium time for the DR-81 adsorption process was found to be approximately 45 minutes, with a maximum removal efficiency of 88.3%. The Zn(II)-MPIH was selected to evaluate its adsorption performance toward the DR-81 from the wastewater.

Three kinetic models were employed to examine the adsorption process. The results, including correlation coefficient values for the linear plots of the three kinetic models for DR-81 ion adsorption onto the Zn(II)-MPIH from aqueous solutions, are summarized in Table 1. The data show that plotting t/q_t *versus* time yields high correlation coefficients for DR-81 (R^2 = 0.999), indicating that the adsorption process follows the second-order kinetic model.[40] Furthermore, the Table 1 reveals that the calculated q_e value for the pseudo-second-order model closely matches the experimental value. These findings confirm that the DR-81 adsorption process is primarily governed by the pseudo-second-order kinetic model for the various water pollutants studied.[7]

2.3.2 Influence of initial pH on the decontamination processes. The pH of the wastewater significantly influences the adsorption process onto the complex. Both the ionization of pollutants and the surface charge of the complex adsorbent are pH-dependent.[41] The adsorption of DR-81 onto the Zn(II)-MPIH complex was investigated across a pH range of 1–11, as shown in Fig. 8a. According to the literature, hydrazone and its complexes exhibit significant chemical stability at different pH values. The ligand itself remains stable even in strongly acidic environments. However, prolonged exposure to a pH of 1 over several hours will lead to its hydrolysis.[42,43] the Adsorption is notably high at a low pH of 3, indicating that the Zn(II)-MPIH exhibits greater adsorption capacity in acidic conditions. The

Table 1 Pseudo-first order, pseudo-second-order, and Elovich kinetic parameters for DR-81 removal onto Zn(II)-MPIH complex

Isotherms	Parameters	Values
Pseudo-first order	q_{exp} (mg g^{-1})	29.17
	q_{theor} (mg g^{-1})	18.87
	K_1 (min^{-1})	0.12
	R^2	0.924
Pseudo-second order	q_{exp} (mg g^{-1})	29.17
	q_{theor} (mg g^{-1})	29.61
	K_2 (g mg^{-1} min^{-1})	0.0023
	R^2	0.999
Elovich kinetic model	q_{exp} (mg g^{-1})	29.17
	α (mg mg^{-1} min^{-1})	84.23
	β (g mg^{-1})	14.17
	R^2	0.971

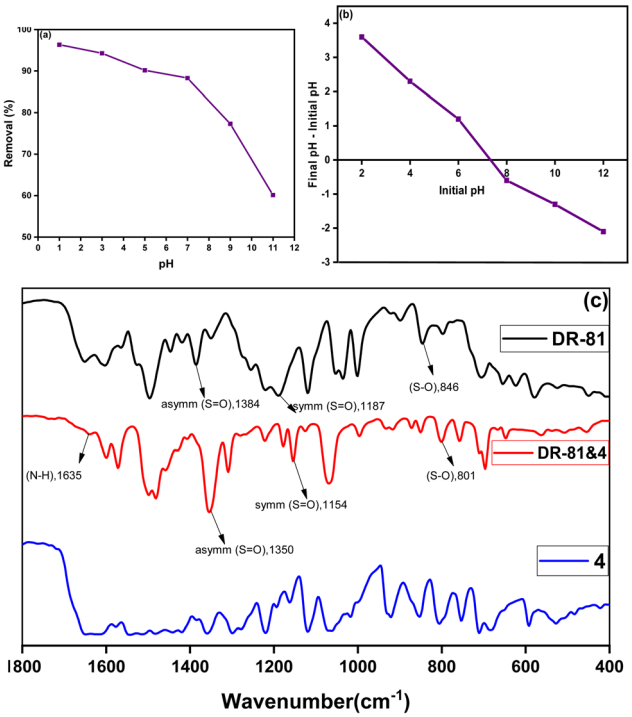

Fig. 8 Effect of pH on DR-81 sorption process onto Zn(II)-MPIH (a), determination of the point of zero charge pH (b) and FT-IR before and after adsorption (c).

adsorption percentage of DR-81 peaks is high at pH 7, then decreases gradually as the pH increases. Fig. 8a illustrates that DR-81 adsorption is more favorable onto the Zn(II)-MPIH under acidic conditions. The adsorption efficiency increases to a maximum of 88.29% at pH 7 but declines to 60.12% at pH 11. Therefore, pH 7 is identified as the optimal pH for DR-81 adsorption onto the Zn(II)-MPIH. The adsorption mechanism at various pH levels can be attributed to the pH at the point of zero charge (pH_{PZC}) of the Zn(II)-MPIH (Fig. 8b) and the molecular nature of DR-81 as an anionic dye.[5] The pH_{PZC} of the adsorbent is 7.3, indicating that the adsorbent surface is positively charged at pH levels below 7.3 and negatively charged above this value. This is supported by the maximum sorption observed for DR-81 at acidic pH levels. When the solution pH drops below the pH_{PZC}, the Zn(II)-MPIH surface becomes positively charged, enhancing the adsorption of DR-81 anions through electrostatic attraction.

The adsorption between the zinc complex and the DR-81 dye was suggested by the electrostatic interaction between the sulfonate group of DR-81 dye and the uncoordinated protonated *N*-pyridine of the complex, by careful comparison of the IR spectra of the complexes with those of the free dye (Fig. 8c). The ν(S–O) band of the free dye appeared at 846 cm^{-1} and shifted to 801 cm^{-1} after adsorption. In addition, the asymmetric ν(S=O) band of the free dye was shifted by −34 cm^{-1} and the symmetric ν(S=O) band of the free dye was shifted by −33 cm^{-1} after adsorption. The appearance of a new ρ(N–H) band at 1635 cm^{-1} indicates that the *N*-pyridine has been protonated. This is consistent with the higher adsorption capacity between the dye and the complex in acidic medium compared to neutral and basic medium because in acidic medium the *N*-pyridine has a positive charge; thus, the adsorption increases with the negatively charged dye.

2.3.3 Effect of the fabricated Zn(II)-MPIH dosage on the decontamination processes. Adsorbent dosage is a crucial parameter because it affects the adsorption capacity of an adsorbent while maintaining a constant initial concentration of the pollutant.[3] The effect of varying Zn(II)-MPIH dosages on both the percentage of DR-81 removal and the material's sorption capacity was evaluated after 45 minutes. As shown in Fig. 9, increasing the Zn(II)-MPIH dosage from 0.25 to 8 g L^{-1} enhanced the removal of DR-81. However, the adsorption capacity per unit of Zn(II)-MPIH decreased with higher dosages. This reduction in adsorption capacity at higher adsorbent dosages may be due to the presence of unoccupied adsorption sites on the Zn(II)-MPIH. Nevertheless, a higher adsorbent dosage provides more active sites for DR-81, thereby improving the removal percentage.[38,39] Consequently, the optimal dosage of Zn(II)-MPIH for DR-81 removal was determined to be 1.0 g L^{-1}.

2.3.4 Effect of initial concentrations of DR-81 on the decontamination processes. The effect of initial DR-81 concentrations on adsorption was investigated over a range of 5 to 200 mg L^{-1}, while maintaining optimal material dosages, contact time, and pH. As illustrated in Fig. 10, the adsorption capacity increased with rising initial concentrations from 5 to 200 mg L^{-1}, consistent with findings from other studies.[44] Initially, a high adsorption rate is observed due to the abundance of active sites on the adsorbent surface. However, as these sites become occupied, the rate slows down. The increase in adsorption capacity with higher initial DR-81 concentrations can be attributed to a larger concentration gradient, which enhances the driving force needed to overcome the resistance to mass transfer of dye ions between the aqueous and solid phases. The optimum initial dye concentration that Zn(II)-MPIH can handle is around 75 ppm, with acceptable dye removal

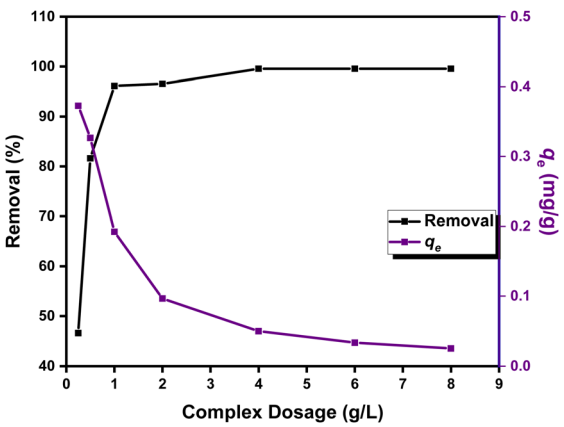

Fig. 9 Effect of Zn(II)-MPIH dosage on both DR-81 percentage adsorption and DR-81 uptake capacity (q_e) (contact time = 45 min, pH = 7, initial DR-81 concentration = 10 ppm, stirring speed = 350 rpm, and temperature = 25 °C).

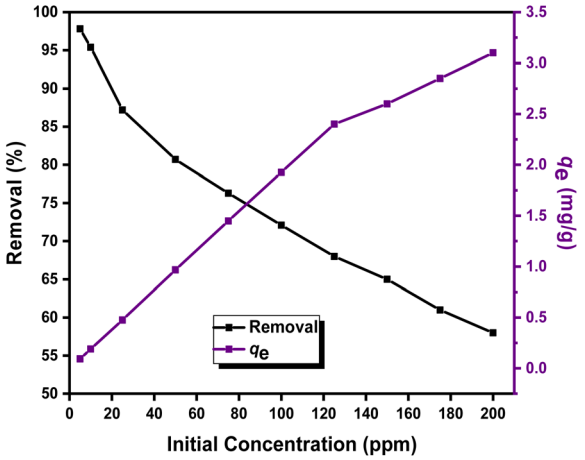

Fig. 10 Effect of initial DR-81 concentration on both the percentage of adsorption and capacity of DR-81 onto Zn(II)-MPIH (contact time = 45 min, pH = 7, complex dosage = 1 g L^{-1}, stirring speed = 350 rpm and temperature = 25 °C).

performance of 76.3%. These results demonstrate that the Zn(II)-MPIH is highly effective for the decontamination of DR-81 from wastewater, regardless of the initial concentration.[7,39]

2.3.5 Effect of solution temperature on the DR-81 decontamination processes. Fig. 11 illustrates the impact of temperature on the removal of DR-81 using the Zn(II)-MPIH. The results indicate that the maximum equilibrium adsorption capacity was achieved at 25 °C. As the temperature rises, the adsorption capacity decreases. This decline is likely due to an increased kinetic energy of the DR-81 molecules at higher temperatures, which reduces their tendency to be adsorbed onto the surface of the complex.[45,46] These findings suggest that the adsorption of DR-81 onto the Zn(II)-MPIH is an exothermic process.

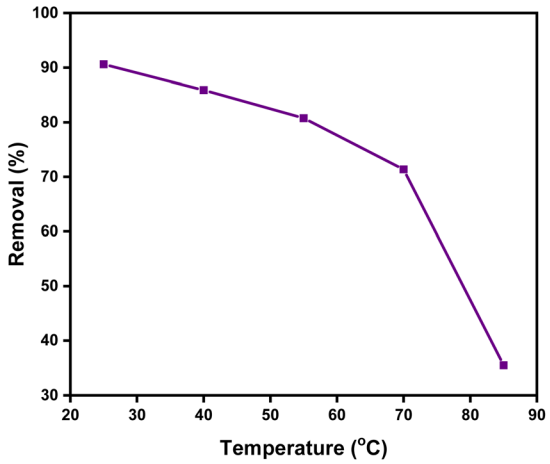

Fig. 11 Effect of DR-81 solution temperature on the percentage of DR-81 removal onto Zn(II)-MPIH (contact time = 45 min, pH = 7, initial DR-81 concentration = 10 ppm, complex dosage = 1 g L^{-1}, and stirring speed = 350 rpm).

2.4 Thermodynamics parameters of the decontamination process of DR-81

To investigate the nature of the adsorption processes, it is essential to determine the standard free energy (ΔG^0), changes in enthalpy (ΔH^0), and entropy (ΔS^0) as key thermodynamic parameters. The standard values for enthalpy and entropy can be calculated using the following eqn (1)–(3).[47]

$$\Delta G = -RT\ln K_d \quad (1)$$

$$\Delta G^0 = \Delta H^0 - T\Delta S \quad (2)$$

$$\ln K_d = \frac{\Delta S^0}{R} - \frac{\Delta H^0}{RT} \quad (3)$$

where the distribution coefficient ($K_d = C_{ad}/C_e$) is a dimensionless parameter representing the ratio of the solute concentration adsorbed on the complex (C_{ad}) to its residual concentration in the solution at equilibrium (C_e). The universal gas constant (R) = 8.314 J mol^{-1} K^{-1}, while T is the solution temperature in Kelvin. The relationship of ln K_d *versus* 1000/T was represented as a straight line with an acceptable value of R^2. ΔH^0 and ΔS^0 values can be detected from the plot slope and the intercept, respectively. All the data are summarized in Table 2. The negative values of ΔG^0 values indicate that the DR-81 decontamination processes on the Zn(II)-MPIH are thermodynamically favorable and spontaneous. Conversely, the negative enthalpy values reflect the exothermic nature of the adsorption processes. Additionally, the negative change in entropy (ΔS^0), suggests a more ordered activation stage, indicating that the adsorption mechanism involves an associative process.[48,49]

2.5 Equilibrium isotherm of the adsorption of DR-81

Three equilibrium models are commonly used to study adsorption processes on various substrates.[50–52] A comparison of the linearization fits for these three models, as detailed in Table 3, reveals that the Freundlich model best represents the pollutant adsorption processes onto the Zn(II)-MPIH. The Freundlich adsorption intensity (n_F) for DR-81 was recorded as 0.763, which is less than unity, indicating that the adsorption processes on the Zn(II)-MPIH are favorable. Consequently, the Freundlich model is the most appropriate for describing the multilayer adsorption of DR-81 on the Zn(II)-MPIH surface. The Langmuir model constants and correlation coefficients are presented in Table 3. A comparison of the correlation coefficients for the Langmuir and Temkin models with that of the

Table 2 Thermodynamic parameters for DR-81 sorption onto Zn(II)-MPIH

Temp. (K)	1000/T	K_e	ln K_e	ΔG^0 (kJ mol^{-1})	ΔH^0 (kJ mol^{-1})	ΔS^0 (J mol^{-1} K^{-1})
298	3.36	1.83	0.60	−11.44	−33.38	−101.32
313	3.19	1.11	0.10	−8.15		
328	3.05	0.74	−0.30	−7.72		
343	2.92	0.39	−1.02	−6.89		
358	2.79	0.14	−1.97	−5.73		

Table 3 Isotherm parameters of Freundlich, Langmuir and Temkin, for DR-81 decontamination onto the Zn(II)-MPIH

Isotherm model	Parameters	Values
Langmuir	q_m (mg g^{-1})	48.311
	k_L (L mg^{-1})	0.212
	R^2	0.801
Freundlich	K_F (mg g^{-1})(L mg^{-1})$^{1/n}$	0.337
	$1/n_F$	1.31
	R^2	0.998
Temkin	A (L g^{-1})	3.873
	B (J mol^{-1})	6.092
	R^2	0.951

Freundlich model shows that the equilibrium data for DR-81 multilayers' adsorption onto the Zn(II)-MPIH align more closely with the Freundlich model.

2.6 Decontamination capacity comparison for the synthesized Zn(II)-MPIH with other adsorbent materials

The multilayer adsorption capacities (q_m) of the Zn(II)-MPIH for DR-81 were compared with those of other similar adsorbent materials, as shown in Table 4. The table clearly demonstrates that the Zn(II)-MPIH offers economically viable and promising results for the adsorption of anionic dyes like DR-81 when compared to other adsorbent nanomaterials reported in the literature.

2.7 Reusability investigation

The adsorption–desorption cycles were repeated eight times. The results demonstrated that the Zn(II)-MPIH could be reused up to five times with satisfactory removal efficiency for DR-81 (>60%), as illustrated in Fig. 12. The decrease in removal efficiency of DR-81 with Zn(II)-MPIH after multiple recycling could be attributed to several factors related to its chemical stability and regeneration process.[3,9] Over multiple cycles, the adsorption sites on Zn(II)-MPIH may become partially blocked or altered, leading to a reduction in its adsorption capacity. This could result from incomplete regeneration during the NaOH treatment and washing steps, where some dye molecules or byproducts may remain bound to the compound, reducing the number of active sites available for further adsorption.[5,6]

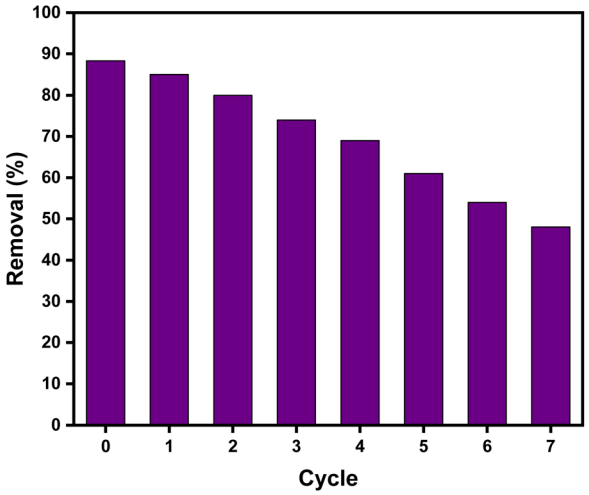

Fig. 12 The adsorption–desorption cycles of DR-81 onto Zn(II)-MPIH.

3. Experimental

3.1 Materials

3-methylpicolinaldehyde (98.0%) and isonicotinic acid (99%) were obtained from Win–Win Chemical CO., Limited., China. Hydrazine hydrate (N_2H_4, 50–60%), $ZnCl_2$, and DR-81 (50% dye content, M. Wt = 675.60 g mol^{-1}) were purchased from Sigma-Aldrich company. All reagents and solvents were used without extra purification.

Table 4 Comparison of adsorption capacities of DR-81 *via* different adsorbent nanomaterials

Pollutant	Adsorbent material	Optimized conditions	Adsorption capacity (mg g^{-1})	Reference
DR-81	Zn(II)-MPIH	Time = 45 min Dosage = 1 g L^{-1} DR-81 conc. = 10 mg L^{-1}	48.31	This study
	Zr-MOF MIP-202	Time = 12 min Dosage = 1 g L^{-1} DR-81 conc. = 10 mg L^{-1}	36.07	7
	Zn Asp MOF	Time = 60 min Dosage = 1 g L^{-1} DR-81 conc. = 10 mg L^{-1}	29.15	5
	Kaolinite	Time = 120 min Dosage = 4 g L^{-1} DR-81 conc. = 50 mg L^{-1}	26.55	53
	Potato peel	Time = 50 min Dosage = 0.25 g L^{-1} DR-81 conc. = 50 mg L^{-1}	10.40	54
	Neem bark	Time = 50 min Dosage = 0.25 g L^{-1} DR-81 conc. = 50 mg L^{-1}	8.40	54

3.2 Characterization methods

The melting points were measured using the Stuart SMP10 (Stuart Scientific, Stone, UK). Homogeneity of the products and follow-up of the reactions was checked by thin layer chromatography (TLC) on plates precoated with silica gel G (Merck; layer thickness 0.25 mm), used without pretreatment. The IR spectra were recorded on a Bruker Vector-22 spectrometer (Bruker Corporation, Billerica, MA, USA). The samples were prepared by suspending them in mineral oil or as thin films, obtained from chloroform solutions dried on the surface of the KBr tablet. The NMR spectra were recorded on Bruker Avance 400 Nanobay (Bruker Corporation, Billerica, MA, USA) with signals from residual protons of deuterated solvents (DMSO-d_6) as the internal standard. Mass spectra were obtained on EI MS electron ionization mass spectrometry (Thermo Scientific, USA, 70 eV). The elemental analysis of the compounds was performed on a Thermo Flash 2000 Elemental Analyzer. The UV-vis spectra were recorded in a quartz cell (light path 10 mm) on a Shimadzu UV-2600 UV-vis spectrophotometer (Shimadzu Corporation, Kyoto, Japan) equipped with a Cary dual-cell Peltier accessory.

3.3 Synthesis

3.3.1 Synthesis of (*E*/*Z*)-*N*′-((3-methylpyridin-2-yl) methylene)isonicotinohydrazide (MPIH) 3. Isonicotinohydrazide **1** (1.37 g, 10 mmol) was added to a solution of 3-methylpicolinaldehyde **2** (1.21 g, 10 mmol) in 30 mL of methanol, and the reaction mixture was refluxed for 4 hours. Using TLC (in dimethyl ether and ethyl acetate = 1 : 1), confirm that the reaction has finished. After cooling the reaction mixture to room temperature, the precipitate that had formed was filtered, washed with water, and dried to produce a white powder.

Yield 89% (2.14 g), mixture of *E* : *Z* isomers = 2 : 1; MP 160–162 °C. R_f 0.7. Anal. calculated for $C_{13}H_{12}N_4O$: C, 65.00; H, 5.00; N, 23.33%. Found: C, 65.11; H, 4.98; N, 23.26%. IR (KBr) ν_{max} cm^{-1}: 3413 (NH), 3108 (CH)$_{aromatic}$, 2853 (CH)$_{azomethine}$, 1671 (C=O), 1633 (C=N)$_{azomethine}$, 1601 (C=N)$_{pyridine}$, 1547, 1490 (C=C) $_{aromatic}$ and 1141 (N–N). ^{1}H NMR (400 MHz, DMSO-d_6, 25 °C), *E* isomer, δ ppm: 12.18–12.13 (d, 1H each, NH or OH); 8.86 (d, 4H, ArH$_1$); 8.75 (d, 2H, ArH$_3$); 8.52 (br.s., 2H, –N=C–H); 7.92 (m, 4H, ArH$_2$); 7.83 (m, 3H, 2 ArH$_4$); 7.51, 7.34 (m, 1H each, ArH$_5$) and 2.56 (s, 6H, 2 CH$_3$). ^{1}H NMR (400 MHz, DMSO-d_6, 25 °C), *Z* isomer, δ ppm: 16.09 (s, 1H, NH); 8.82 (d, 2H, ArH$_1$); 8.65 (d, 1H, ArH$_3$); 7.85 (m, 2H, ArH$_2$); 7.83 (m, 3H, 1 ArH$_4$); 7.72 (d, 1H, ArH$_5$); 7.62 (br.s., 1H, –N=C–H) and 2.52 (s, 3H, CH$_3$). ^{13}C NMR (101 MHz, DMSO-d_6), mixture of *E* and *Z* isomers, δ ppm: 18.39 (CH$_3$), 20.67 (CH$_3$), 121.46 (C$_{Ar}$), 122.06 (C$_{Ar}$), 123.07 (C$_{Ar}$), 123.92 (C$_{Ar}$), 124.15 (C$_{Ar}$), 125.43 (C$_{Ar}$), 132.94 (C$_{Ar}$), 133.78 (C$_{Ar}$), 135.58 (C$_{Ar}$), 137.70 (C$_{Ar}$), 139.80 (C$_{Ar}$), 140.45 (C$_{Ar}$), 140.82 (C$_{Ar}$), 140.96 (C$_{Ar}$), 146.13 (C$_{Ar}$), 147.36 (C$_{Ar}$), 147.47 (C$_{Ar}$), 148.06 (C$_{Ar}$), 149.97 (N=CH), 150.11 (N=CH), 150.59 (C$_{Ar}$), 150.86 (C$_{Ar}$), 151.43 (C$_{Ar}$), 162.00, 162.27, 169.18 (keto and enolate groups) ppm.

3.3.2 Zn(II)-MPIH complex 4. An aqueous solution of $ZnCl_2$ (136 mg, 1 mmol) was added in portions to a magnetically stirred solution of MPIH **3** (240 mg, 1 mmol) containing 3 drops of triethylamine in methanol. The precipitate was filtered off and washed with methanol. Yield: 54.1%. MP > 300 °C. EI-MS [$C_{26}H_{22}O_2N_8Zn$] calculated/found (*m*/*z*) = 542.12, 542.32 and [$C_{17}H_{19}O_2N_8Zn$] calculated/found (*m*/*z*) = 431.09, 431.42. IR (KBr cm^{-1}) selected bands: ν(C–O) 1358; ν(C=N) 1646, 1615; ν(C=N$_{py}$) 1575; ν(N–N) 1068; ρ(py) 710; ν(M–O) 593; ν(M–N) 528.^{1}H NMR (400 MHz, DMSO-d_6, 25 °C), δ ppm: 9.01, 8.84 (2s, 1H each, ArH$_1$), 8.72 (d, J = 5.1 Hz, 2H, ArH$_1$), 8.67 (d, J = 6.2 Hz, 1H, ArH$_3$), 8.63 (d, J = 5.1 Hz, 1H, ArH$_3$), 8.54–8.25 (2 br.s., 1H each, –N=C–H); 8.06 (d, J = 5.1 Hz, 2H, ArH$_2$), 8.01 (d, J = 6.2 Hz, 1H, ArH$_2$), 7.93 (d, J = 7.8 Hz, 1H, ArH$_2$), 7.86–7.78 (m, 2H, ArH$_4$), 7.54 (br.s., 1H, ArH$_5$), 7.44–7.30 (m, 1H, ArH$_5$), 2.56 (d, J = 6.2 Hz, 6H, 2 CH$_3$). ^{13}C NMR (101 MHz, DMSO-d_6, 25 °C) δ ppm: 173.14, 172.87 (C–O), 146.98, 146.75 (N=CH), 150.26, 150.19, 150.11, 145.18, 144.20, 142.27, 142.15, 140.83, 134.85, 134.69, 126.23, 124.02, 122.62, 122.53, 122.31, (C$_{Ar}$), 16.98, 16.91 (CH$_3$).

3.4 Batch decontamination of DR-81 from aqueous media

The batch adsorption technique was used to evaluate the adsorption performance of the synthesized Zn(II)-MPIH for the removal of DR-81 dye from wastewater. In this process, 10 mg of Zn(II)-MPIH was mixed with 100 mL of DR-81 solution at different initial concentrations, maintaining a temperature of 25 °C and a stirring speed of 350 rpm using a shaking incubator. The study assessed the Zn(II)-MPIH adsorption performance through several process parameters: contact time (0–180 minutes), pH (1–11), adsorbent dosage (0.25–8 g L^{-1}), initial pollutant concentration (5–100 mg L^{-1}), and reaction temperature (25–85 °C). All adsorption experiments were conducted in triplicate, and the mean values were used for data analysis to ensure reliability. After the treatment, the final DR-81 concentration was determined by separating the precipitated adsorbent material *via* centrifugation, followed by colorimetric analysis using a UV spectrophotometer at 465 nm. The percentage of pollutant removal by Zn(II)-MPIH was calculated using eqn (4):

$$\text{Removal}\% = \frac{C_o - C_e}{C_o} \times 100 \quad (4)$$

where C_o is the initial concentration of the pollutant (mg L^{-1}), and C_e is the pollutant concentration at equilibrium in the aqueous solution (mg L^{-1}). The adsorption capacity of the pollutant (mg g^{-1}) was calculated using eqn (5):

$$q_e = \frac{V(C_o - C_e)}{m} \quad (5)$$

where q_e is the adsorption capacity (mg g^{-1}), V is the volume of the solution (L), and m is the mass of the Zn(II)-MPIH (g).

3.5 Equilibrium, kinetics, and thermodynamics of DR-81 adsorption onto Zn(II)-MPIH

The thermodynamic parameters of the adsorption process for DR-81 dye were assessed. Additionally, the equilibrium behavior of the adsorption process was evaluated using the

Langmuir, Freundlich, and Temkin isotherm models to determine the relationship between the adsorption of DR-81 onto the Zn(II)-MPIH and its equilibrium concentration in water. The Langmuir model assumes that adsorption is monomolecular and occurs on a homogeneous surface, where all adsorption sites have identical affinities for the adsorbate. In contrast, the Freundlich isotherm model applies to heterogeneous surfaces with multilayer adsorption (eqn (6) and (7)).

$$\frac{C_e}{q_e} = \frac{1}{q_m K} + \frac{C_e}{q_m} \quad (6)$$

where q_e (mg g^{-1}) is the amount of adsorbate adsorbed at equilibrium, C_e (mg L^{-1}) is the equilibrium concentration of DR-81, and K_L and q_m are the Langmuir constant and the capacity related to maximum adsorption, respectively. Additionally, eqn (4) was used to evaluate the Freundlich model.

$$\log q_e = \log k_F + \frac{1}{n_F} \log C_e \quad (7)$$

where k_F (mg g^{-1}) is the Freundlich adsorption capacity constant, and n_F is a dimensionless exponent of the Freundlich equation. The sorption data of DR-81 onto the Zn(II)-MPIH were analyzed using the Temkin isotherm model as described in eqn (8):

$$q_e = B \ln A + B \ln C_e \quad (8)$$

where A is the Temkin isotherm constant (L g^{-1}), and $B = RT/b$ is the constant related to the heat of adsorption (J mol^{-1}). To explore the nature of the adsorption processes, the kinetics of DR-81 adsorption onto Zn(II)-MPIH were analyzed using both pseudo-first-order and pseudo-second-order kinetic models. The pseudo-first-order kinetic model is described by eqn (9):

$$\ln(q_e - q_t) = \ln q_e - k_1 t \quad (9)$$

where q_e (mg g^{-1}) is the amount of DR-81 adsorbed at equilibrium, q_t (mg g^{-1}) is the amount of DR-81 adsorbed at any time t (h), and k_1 (h^{-1}) is the adsorption rate constant. The pseudo-second-order constants were determined using eqn (10).

$$\frac{t}{q_t} = \frac{1}{k_2 q_2} + \frac{t}{q} \quad (10)$$

where: k_2 (g mg^{-1} h^{-1}) is the pseudo-second-order rate constant. Following this, the Elovich equation was applied for the adsorption of various water pollutants, as represented by eqn (11):

$$q_t = \alpha + \beta \ln t \quad (11)$$

where α represents the initial adsorption rate (mg g^{-1} min^{-1}), and β is associated with the degree of surface coverage and the activation energy of the adsorption (g mg^{-1}). Both α and β can be determined from the linear plot of q_t against $\ln t$, using the slope and intercept of the plot.

3.6 Reusability of the fabricated Zn(II)-MPIH

To enhance the economic feasibility of water treatment processes, the Zn(II)-MPIH adsorbent was regenerated ten times. For this, 1.0 g of Zn(II)-MPIH was suspended in 100 mL of 0.01 M NaOH solution and stirred at 350 rpm for 24 hours. The regenerated material was then washed twice with deionized water and once with ethanol, before being dried at 70 °C overnight for subsequent reuse.

4. Conclusions

In conclusion, we present for the first time an efficient adsorbent in the form of a porous Zn(II)-MPIH complex. The synthesized Zn(II)-MPIH was thoroughly characterized using ^{1}H NMR, ^{13}C, FT-IR, UV-visible and EI MS. The adsorption behavior of DR-81 was best described by the Freundlich model, indicating multilayer adsorption on the Zn(II)-MPIH. The pseudo-second-order model was identified as the most suitable kinetic model for the adsorption process. The optimum dosage of the Zn(II)-MPIH complex was found to be 1.0 g L^{-1} at a pH of 7, resulting 88.3% adsorption of 10 ppm DR-81 in 45 minutes at 25 °C. Moreover, the maximum adsorption capacity of the Zn(II)-MPIH for DR-81 was 48.3 mg g^{-1}. The decontamination performance was 88.3%, 85.6%, 80.1%, 74.7, 69.9%, 61.8% and 54.9% after seven repetitive rounds using Zn(II)-MPIH. Moreover, this material proves to be an effective and promising adsorbent for DR-81 removal from aqueous solutions, showing high stability and the ability to be recycled for up to five cycles, with easy regeneration of the sorbent.

Data availability

The authors confirm that the data supporting the findings of this study are available within the article.

Author contributions

All authors contributed to the design of experiments. Conceptualization, Mohamed A. Ahmed, Eslam Salama, and Mohamed A. Khalifa; investigation and data curation, Mohamed A. Ahmed, Eslam Salama, M. H. H. Mahmoud, Mohamed Ebaid, and Mohamed A. Khalifa; writing – original draft preparation, Mohamed A. Ahmed, Eslam Salama and Mohamed A. Khalifa; writing – review and editing, Mohamed A. Ahmed, Eslam Salama and Mohamed A. Khalifa; project administration, all authors have read, reviewed, and agreed to the published version of the manuscript.

Conflicts of interest

The authors declare no conflict of interest.

Acknowledgements

The authors extend their appreciation to Taif University, Saudi Arabia, for supporting this work through project number (TU-DSPP-2024-93).

Notes and references

1 B. Stewart-Koster, S. E. Bunn, P. Green, C. Ndehedehe, L. S. Andersen, D. I. Armstrong McKay, X. Bai, F. DeClerck, K. L. Ebi and C. Gordon, *Nat. Sustain.*, 2024, **7**, 53–63.

2 G. Saxena, R. Chandra and R. N. Bharagava, *Rev. Environ. Contam. Toxicol.*, 2017, **240**, 31–69.

3 N. Meky, E. Salama, M. F. Soliman, S. G. Naeem, M. Ossman and M. Elsayed, *Water, Air, Soil Pollut.*, 2024, **235**, 154.

4 E. Salama, M. Samy, H. S. Hassan, S. Mohamed, K. Mensah and M. F. Elkady, *Environ. Sci. Pollut. Res.*, 2024, **31**, 44863–44884.

5 E. Salama, M. Ghanim, H. S. Hassan, W. A. Amer, E.-Z. M. Ebeid, A. H. El-Shazly, M. Ossman and M. F. Elkady, *RSC Adv.*, 2022, **12**, 18363–18372.

6 E. Salama, A. Hamdy, H. S. Hassan, W. A. Amer, E.-Z. M. Ebeid, M. Ossman and M. F. Elkady, *Adsorpt. Sci. Technol.*, 2022, **2022**, 6818348.

7 K. E. Diab, E. Salama, H. S. Hassan, A. Abd El-moneim and M. F. Elkady, *Sci. Rep.*, 2021, **11**, 1–13.

8 L. Handojo, D. Pramudita, D. Mangindaan and A. Indarto, *Emerging Eco-Friendly Green Technologies for Wastewater Treatment*, 2020, pp. 45–76.

9 E. Salama, M. Ossman, A. Hamdy, H. Shokry and M. F. Elkady, *AIP Adv.*, 2023, **13**, 025349.

10 G. Mahmoudi, H. Chowdhury, B. K. Ghosh, M. Kubicki, A. Bartyzel, J. M. White, I. Alkorta, A. V. Gurbanov and D. A. Safin, *J. Molec. J. Mol. Struct.*, 2021, **1229**, 129614.

11 Y. Burgos-López, L. M. Balsa, O. E. Piro, I. E. León, J. García-Tojal, G. A. Echeverría, A. C. González-Baró and B. S. Parajón-Costa, *Polyhedron*, 2022, **213**, 115621.

12 D. Shobana, S. Sudha, D. Ramarajan and D. Dimić, *J. Mol. Struct.*, 2022, **1250**, 131856.

13 G. M. Al-Daher and T. Y. Yousif, *Rafidain J. Sci.*, 2017, **26**, 38–48.

14 Y. Li, Z. Yang, M. Zhou, Y. Li, J. He, X. Wang and Z. Lin, *RSC Adv.*, 2017, **7**, 41527–41539.

15 F. Borbone, U. Caruso, R. Centore, A. De Maria, A. Fort, M. Fusco, B. Panunzi, A. Roviello and A. Tuzi, *Eur. J. Inorg. Chem.*, 2004, **2004**, 2467–2476.

16 H.-J. Liu, R. Yi, D.-M. Chen, C. Huang and B.-X. Zhu, *Molec*, 2020, **26**, 109.

17 M. Jabeen, *J. Turk. Chem. Soc., Sect. A*, 2022, **9**, 663–698.

18 M. Sutradhar, T. Roy Barman, A. J. Pombeiro and L. M. Martins, *Int. J. Mol. Sci.*, 2020, **21**, 2832.

19 D. K. Chelike, A. Alagumalai, V. Muthukumar, S. A. G. Thangavelu and A. Krishnamoorthy, *New J. Chem.*, 2020, **44**, 13401–13414.

20 S. Sathiyakumar, P. Selvam, F. L. Hakkim, K. Srinivasan and W. T. Harrison, *J. Coord. Chem.*, 2018, **71**, 3521–3533.

21 X. Huang, S.-Y. Yan, Y.-M. Chen, D.-S. Zhang, C. Huang, B.-X. Zhu and J.-H. Lu, *Inorg. Chim. Acta.*, 2023, **555**, 121588.

22 K.-J. Wang, R.-H. Gao, Y. Fan, C. Huang, B.-X. Zhu and J.-H. Lu, *Inorg. Chim. Acta*, 2024, 122208.

23 D.-M. Chen, X.-F. Wu, Y.-J. Liu, C. Huang and B.-X. Zhu, *Inorg. Chim. Acta.*, 2019, **494**, 181–186.

24 N. V. Shtyrlin, R. M. Khaziev, V. G. Shtyrlin, E. M. Gilyazetdinov, M. N. Agafonova, K. S. Usachev, D. R. Islamov, A. E. Klimovitskii, T. I. Vinogradova and M. Z. Dogonadze, *Med. Chem. Res.*, 2021, **30**, 952–963.

25 N. Y. Subbaiah, S. K. Mohanty, B. N. Sudha and C. Ayyanna, *Synthesis*, 2016, **1**, 39–42.

26 D. S. Cukierman, E. Accardo, R. G. Gomes, A. De Falco, M. C. Miotto, M. C. R. Freitas, M. Lanznaster, C. O. Fernández and N. A. Rey, *JBIC, J. Biol. Inorg. Chem.*, 2018, **23**, 1227–1241.

27 E. L. Romero, R. F. D'Vries, F. Zuluaga and M. N. Chaur, *J. Braz. Chem. Soc.*, 2015, **26**, 1265–1273.

28 F. Martins, S. Santos, C. Ventura, R. Elvas-Leitão, L. Santos, S. Vitorino, M. Reis, V. Miranda, H. F. Correia and J. Aires-de-Sousa, *Eur. J. Med. Chem.*, 2014, **81**, 119–138.

29 P. H. Santiago, M. B. Santiago, C. H. Martins and C. C. Gatto, *Inorg. Chim. Acta.*, 2020, **508**, 119632.

30 M. A. Ahmed, M. A. Zhernakov, E. M. Gilyazetdinov, M. S. Bukharov, D. R. Islamov, K. S. Usachev, A. E. Klimovitskii, N. Y. Serov, V. A. Burilov and V. G. Shtyrlin, *Inorganics*, 2023, **11**, 167.

31 N. A. Mangalam and M. P. Kurup, *Spectrochim. Acta, Part A*, 2011, **78**, 926–934.

32 N. A. Mangalam, S. Sivakumar, M. P. Kurup and E. Suresh, *Spectrochim. Acta, Part A*, 2010, **75**, 686–692.

33 Y. Li, Z. Yang, M. Zhou, J. He, X. Wang, Y. Wu and Z. Wang, *J. Molec. J. Mol. Struct.*, 2017, **1130**, 818–828.

34 M. Bashir, A. A. Dar and I. Yousuf, *ACS Omega*, 2023, **8**, 3026–3042.

35 A. A. Khandar, F. A. Afkhami, S. A. Hosseini-Yazdi, J. Lipkowski, W. G. Dougherty, W. S. Kassel, H. R. Prieto and S. García-Granda, *J. Inorg. Organomet. Polym. Mater.*, 2015, **25**, 860–868.

36 C. Anitha, S. Sumathi, P. Tharmaraj and C. Sheela, *Int. J. Inorg. Chem.*, 2011, **2011**, 493942.

37 J. K. CHAVAN and R. PATIL, *Orient. J. Chem.*, 2024, **40**, 3.

38 M. F. Elkady, H. S. Hassan, W. A. Amer, E. Salama, H. Algarni and E. R. Shaaban, *Materials*, 2017, **10**, 1355.

39 M. F. Elkady, H. Shokry Hassan and E. Salama, *J. Eng.*, 2016, **2016**, 2308560.

40 A. B. Botelho Junior, É. F. Pinheiro, D. C. R. Espinosa, J. A. S. Tenório and M. d. P. G. Baltazar, *Sep. Sci. Technol.*, 2022, **57**, 60–69.

41 H. Shokry, M. Elkady and E. Salama, *Sci. Rep.*, 2020, **10**, 1–17.

42 D. Richardson, L. W. Vitolo, E. Bakers and J. Webb, *Biol. Met.*, 1989, **2**, 69–76.

43 T. Zamzam, S. Jadhav, D. Kayande and R. Megha, *Int. J. Curr. Pharmaceut. Res.*, 2019, **407**, 58–65.

44 K. E. Diab, E. Salama, H. S. Hassan, A. A. El-moneim and M. F. Elkady, *Polymers*, 2021, **13**, 3869.

45 M. Saghian, S. Dehghanpour and M. Sharbatdaran, *RSC Adv.*, 2020, **10**, 9369–9377.

46 O. L. Uyanika, N. Bektasb and N. Uyanikb, *Int. J. Appl. Eng. Res.*, 2018, **13**, 11112–11122.

47 W. Huang, K. Diao, X. Tan, F. Lei, J. Jiang, B. A. Goodman, Y. Ma and S. Liu, *Polymers*, 2019, **11**, 969.

48 M. Elkady, E. Salama, W. A. Amer, E.-Z. M. Ebeid, M. M. Ayad and H. Shokry, *Environ. Sci. Pollut. Control Ser.*, 2020, **27**, 43077–43092.
49 T. Ngulube, J. R. Gumbo, V. Masindi and A. Maity, *Clay Miner.*, 2019, **54**, 197–207.
50 W. A. Amer, M. M. Omran, A. F. Rehab and M. M. Ayad, *RSC Adv.*, 2018, **8**, 22536–22545.
51 S. Zaghlol, W. A. Amer, M. H. Shaaban, M. M. Ayad, P. Bober and J. Stejskal, *Chem. Pap.*, 2020, **74**, 3183–3193.
52 W. A. Amer, M. M. Omran and M. M. Ayad, *Colloids Surf., A*, 2019, **562**, 203–212.
53 T. A. Khan, S. Dahiya and E. A. Khan, *Environ. Prog. Sustain. Energy*, 2017, **36**, 45–58.
54 N. Sharma, D. Tiwari and S. Singh, *Rasayan J. Chem.*, 2014, **7**, 399–409.